INFLUENCE OF SILICON CHARACTERISTICS ON THE PARAMETERS OF MANUFACTURED PHOTONICS CELLS

Mykola S. Kukurudziak[a,b]*, **Volodymyr M. Lipka[a,b]**

a Rhythm Optoelectronics Shareholding Company, Holovna str. 244, 58032, Chernivtsi, Ukraine
b Yuriy Fedkovych Chernivtsi National University, Kotsyubyns'kogo str. 2, 58012, Chernivtsi, Ukraine
*Corresponding Author e-mail: mykola.kukurudzyak@gmail.com

The paper investigates the influence of the electrophysical characteristics of silicon on the final parameters of photoelectronic elements using *p-i-n* photodiodes as an example. It has been found that photodiode samples made on the basis of silicon with a higher resistivity are more prone to the formation of inversion channels at the oxide-semiconductor interface. Also, the dark current and responsivity of such photodiodes reach saturation at a lower voltage. It has also been shown that silicon-based photodiodes with a longer lifetime of non-basic charge carriers have lower dark current values. It has been shown that products with crystallographic orientation [111] have a much lower density of surface dislocations after technological operations than in the case of silicon with orientation [100]. It was also found that materials with different crystallographic orientations have different phosphorus diffusion coefficients. It has been experimentally established that a silicon oxide film grows faster on the surface of crystallographic orientation silicon [111] than on the surface of crystallographic orientation silicon [100]. This is due to the difference in the surface density of silicon atoms inherent in different crystallographic planes.
Keywords: *Silicon; Photodiode; Responsivity; Dark current; Dislocations; Crystallographic orientation*
PACS: 61.72.Ji, 61.72.Lk, 85.60.Dw

Semiconductor photovoltaic devices with *p-n* junctions are becoming increasingly popular. For example, they are used in automation, telemechanics, various protective devices, control and measuring equipment, surveillance and guidance circuits, etc. [1]. The emergence of new and improved sources of monochromatic radiation modulated by frequencies in the hundreds and thousands of megahertz, as well as new types of photoelectric semiconductor devices capable of converting an optical signal into an electrical signal, has made it possible to realize many tasks of opto- and photoelectronics.

In recent decades, researchers have paid special attention to the development and production of photodetectors for near-infrared spectral range detection. The manufacture of perfect photo receivers (PR) for this wavelength region remains an urgent scientific and technical task. One of the first issues to be solved in the design and manufacture of photodetectors is the choice of the base semiconductor material. Today, the most commonly used photodetectors are *p-n* junction photodetectors based on A_3B_5 compounds, in particular GaAs, as well as Ge or Si. The choice of material depends primarily on the type of their spectral resposivity characteristic. For example, for wide-band GaAs (E_g =1.42 eV), the spectral response shifts towards short wavelengths, since photons with higher energy (short-wave radiation) are required to create electron-hole pairs and, accordingly, the photocurrent [2]. For semiconductors with a small band gap, such as Ge (E_g = 0.66 eV), the spectral response is shifted to the long-wave region (λ_m=1.54 μm) [3, 4]. In narrow bandgap semiconductors, electron-hole pairs can occur under the influence of photons with lower energy (long-wave radiation).

The dependence of the light absorption coefficient on the wavelength has an impact on the appearance of the spectral response and the location of the maximum. For semiconductors with a sharp dependence of the absorption coefficient on the wavelength (Ge), the maximum of the spectral response for different types of devices usually occurs at the same wavelength regardless of the technology. For semiconductors with a less sharp dependence of the absorption coefficient, such as Si, the maximum spectral response, depending on the design of the photodetector and the technology used, can vary in a wide range from λ=0.6 μm up to the intrinsic absorption edge of λ=1.1 μm [5].

Comparing the capabilities of Si and GaAs materials, we can see that the main influence on the spectral characteristic is due to differences in the mechanism of light absorption. GaAs is characterized by a sharp edge of the main absorption band and a weak dependence of the absorption coefficient on the wavelength in the range of λ=0.4 - 0.9 μm. In this regard, in GaAs photonics cells, the photocurrent value is determined mainly by the base (depth of the *p-n* junction) of the device. Therefore, by changing the thickness of the base, it is possible to change the shape of the spectral response of these photodetectors. In turn, for silicon PRs, the shift in the maximum of the spectral response can be realized both by changing the thickness of the base and by changing the diffusion lengths of non-main charge carriers in the base. By keeping the thickness of the silicon photo receivers base constant and changing the diffusion length of non-basic charge carriers in the source material, it is possible to change the maximum of the spectral curve both in absolute value and in wavelength. The described capabilities of silicon photodetectors to detect wavelengths of a wide range have led to their widespread use in solving photoelectronics problems. In addition to the above, important factors in the use of silicon as the main

material not only for photoelectronics but also for solid-state electronics in general are its widespread use and high manufacturability [6, 7]. In particular, silicon ranks second in terms of its prevalence on Earth: about 27.6 % of the mass of the Earth's crust, about 17 % of the mass of the lithosphere, and about 7 % of the mass of the core (Fig. 1). Note that the mass fraction of silicon in the universe is less than 0.1% [8].
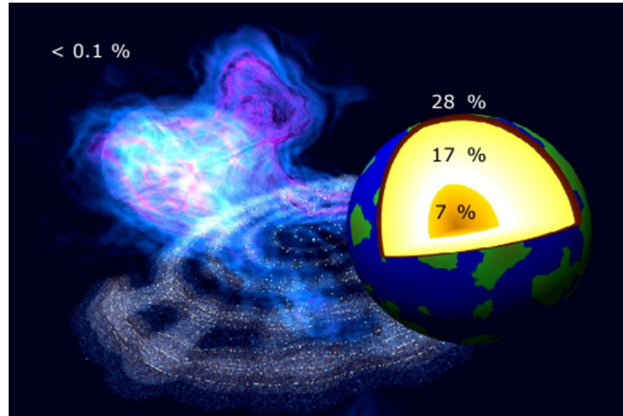

Figure 1. The abundance (in mass %) of silicon in the universe and in the planet Earth

It should be noted that the choice of the base material for the manufacture of photodetectors is not limited to the choice of semiconductor, as there are a number of other parameters of semiconductor ingots or wafers that should be taken into account when designing. These parameters include the type of conductivity, resistivity, density of structural defects, lifetime of minority charge carriers, crystallographic orientation, etc. The ability to estimate the requirements of material parameters, in particular silicon, for the manufacture of specific types of photodetectors is an important and relevant scientific and technical task. A review of the literature shows that most of the works are devoted to the production of defect-free silicon ingots [9], and the influence of growth or acquired defects in the semiconductor material on the parameters of the resulting electronics elements [10, 11]. Also, many works are devoted to the study of technological processes or modes on the parameters of final products, but no works on the influence of the parameters of the source silicon on the parameters of the final photodetectors have been found. Accordingly, the aim of this work is to study the dependence of the final parameters of silicon photodiodes on the electrophysical characteristics of the source silicon.

EXPERIMENTAL

The research was carried out on the example of silicon four-element *p-i-n* photodiodes (PD) with guard ring (GR) designed to detect radiation with a wavelength of λ_{op}=1064 nm. Two different materials with different electrophysical parameters were chosen for comparison. The first material was single-crystal dislocation-free *p*-type FZ-Si with orientation [111], resistivity at $\rho\approx$16-20 k$\Omega\cdot$cm and life time of minority charge carriers at $\tau\approx$1.1-1.3 ms (PD[111]). Another material was single-crystal dislocation-free *p*-type FZ-Si with orientation [100], resistivity at $\rho\approx$45-55 k$\Omega\cdot$cm and life time of minor charge carriers at $\tau\approx$2.2-2.4 ms (PD[100]). The devices were prepared using diffusion planar technology in a single process cycle under the same conditions. The PDs technological route consisted of a complex of four thermal operations and three photolithographies: semiconductor substrates were oxidized according to the principle of dry-wet-dry oxidation; photolithography was carried out to create windows for phosphorus diffusion; diffusion of phosphorus (predeposition) to the front side to create n^+-type responsive elements (RE) and GR; driving-in of phosphorus to redistribute the alloying impurity and increase the depth of the n^+-p junction; diffusion of boron to the reverse side of the substrate to create a p^+-type ohmic contac; photolithography for creating contact windows; sputtering of Cr-Au on the front and back sides, separation of pastes into crystals by scraping or cutting with a disk with an external diamond edge. The thickness of the final photodiode crystals reached 390-400 microns. The parameters of the obtained devices were compared.

After oxidation and each subsequent thermal operation, the high-frequency volt-farad (*C-V*) characteristics of the metal-oxide-semiconductor-strctures were measured at a frequency of 30 kHz, which made it possible to predict the final parameters of the products.

An important parameter of multi-element PDs with GR is the resistance of the isolation of the REs and the GR (R_{con}), the decrease of which leads to an increase in the photocoupling coefficient and dark currents. This parameter characterizes the presence of inversion conduction channels at the Si-SiO$_2$ interface. Determination of insulation resistance of REs and GR was carried out according to the method given in [3] with U_{bias}=2 V and load resistance R_l=10 kΩ.

The dark current (I_d) and *I–V* characteristics of PDs were measured using a hardware-software complex implemented on the basis of the Arduino platform, an Agilent 34410A digital multimeter and a Siglent SPD3303X programmable power source, which were controlled by a personal computer using software created by the authors in the LabView environment (dark current density J_d is given).

Monitoring of current monochromatic pulse responsivity (S_{pulse}) was carried out by method of comparing responsivity of the investigated PD with a reference photodiode certified by the respective metrological service of the company. Measurements were performed when illuminating the PD with a radiation flux of a power of not over $1 \cdot 10^{-3}$ W; load resistance across the responsive element $R_l = 10$ kΩ, at the bias voltages of $U_{bias} = 2\text{-}120$ V and pulse duration $\tau_i = 500$ ns. The spectral characteristics of photodiode responsivity ($S(\lambda)$) at different bias voltages are also obtained. The measurement was carried out using the KSVU-23 automated spectral complex.

The capacitance of REs (C_{RE}) was determined at a $U_{bias} = 2\text{-}120$ V

To investigate the defective structure of the substrates with [111] orientation, chemical treatment was performed in selective Sirtle's etchant [12] with the following composition:

$$HF - 100 \text{ cm}^3, CrO_3 - 50 \text{ g}, H_2O - 120 \text{ cm}^3$$
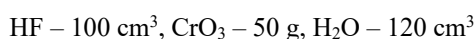
To investigate the defective structure of the substrates with [100] orientation, chemical treatment was performed in selective Secko's etchant [13] with the following composition:

$$4.4\% \text{ K}_2\text{Cr}_2\text{O}_7 : HF = 1 : 2$$
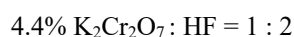
Then the surface was examined in microscopes of different magnifications. The number of dislocations was calculated by the metallographic method [14].

The growth rate of SiO_2 on substrates of different crystallographic orientation has been investigated. The thickness of the oxide films was measured by the ellipsometric method. The depth of the diffusion layer (x_{n+-p}) of phosphorus was also compared at the same diffusion durations. Determination of the depth of the *p-n* junction was performed by spherical grinding.

RESULTS OF THE RESEARCH AND THEIR DISCUSSION
A) Study of *C-V* characteristics and insulation resistance between responsive elements and guard ring

As mentioned above, *C-V* characteristics were monitored after each thermal operation. After thermal oxidation and subsequent heat treatments, the silicon substrates with lower resistivity ($PD_{[111]}$) had a classic volt-faradic characteristic curve for *p*-type material (Fig. 2, curve 1). As for the substrates with a higher resistivity ($PD_{[100]}$), a slight inverted characteristic curve was observed after the first thermal operation (Fig. 2, curve 2). After boron diffusion, a complete inverted *C-V* characteristics was observed (Fig. 2, curve 3).
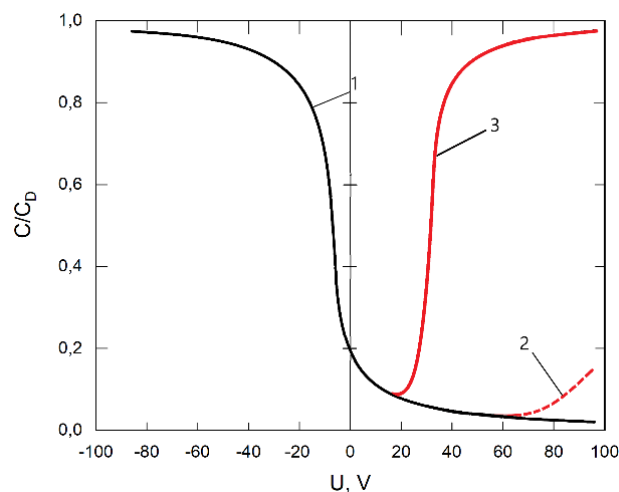

Figure 2. *C-V* characteristics of PDs:
1 - characteristic of $PD_{[111]}$; 2 - characteristic of $PD_{[100]}$ after oxidation; 3 - characteristic of $PD_{[100]}$ after diffusion of boron

The inversion of the *C-V* characteristics indicated the presence of inversion layers at the Si-SiO₂ interface. Technological reasons for the appearance of inversion layers are improper chemical treatment of substrates, the presence of alkali metal impurities in deionized water, quartz dishes, or a quartz reactor and carrier gases. The deterioration of the characteristics after boron diffusion is caused by the redistribution and diffusion of impurities in SiO_2 to the Si-SiO₂ interface introduced during thermal operations due to the high total duration of heat treatment [15, 16]. Silicon for $PD_{[100]}$ is more prone to the formation of inversion layers, since in this case a smaller amount of impurity is required to change the surface conductivity to the opposite one, unlike a material with a lower resistivity.

The parameter that is a vivid quantitative characteristic of the presence of conductive inversion channels at the Si-SiO₂ interface is R_{con}. Measurements showed that samples $PD_{[111]}$ had $R_{con} \approx 3.9\text{-}5.5$ MΩ and samples $PD_{[100]}$ had $R_{con} \approx 0.7\text{-}1.1$ MΩ. As indicated above, R_{con} of $PD_{[100]}$ is much lower than of $PD_{[111]}$, as evidenced by the *C-V*-characteristics. In case of difficulty or impossibility of manufacturing PDs with low R_{con} due to the formation of

surface inversion channels, it is worth forming surface areas of leakage channel restriction isotypic with the substrate material between the REs and GR of the photodiodes [17]. This is especially important when using silicon with a $\rho \geq 20$ kΩ.

B) Study of dark currents of photodiodes

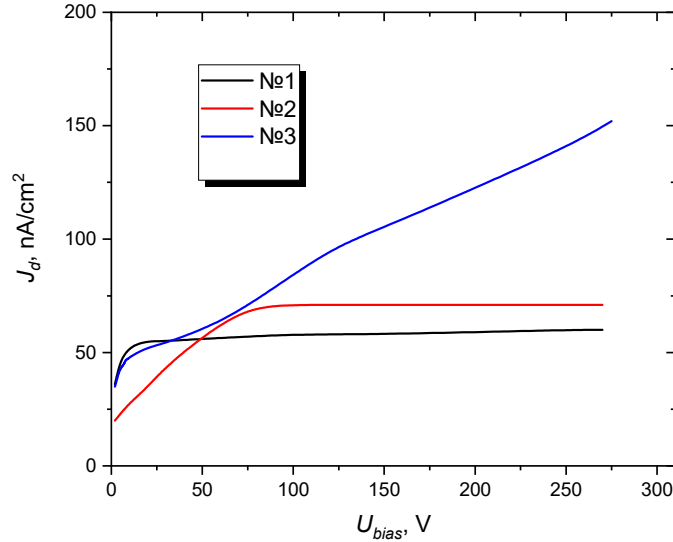The *I-V*-characteristics of photodiodes were obtained (Fig. 3).

Figure 3. *I-V*-characteristics of PDs: 1, 3 - characteristic of PD[100]; 2 - characteristic of PD[111]

The volt-ampere characteristic curves for PD[111] were typical for all samples from the experimental batch with some variation in J_d (curve 1, Fig. 3). The dark currents for PD[111] at U_{bias}=2 V reached J_d =52-78 nA/cm², and at U_{bias}=120 V J_d =156-208 nA/cm².

In the case of PD[100], a slightly different picture was observed. For some PDs, the characteristic of curve type 1 of Fig. 3 was inherent, and for the other part, the characteristic of curve type 3 of Fig. 3. As for the samples with the *I-V*-characteristic of curve type 1, in this case, the value of the dark current reached slightly lower values than in PD[111] (at voltages above the saturation voltage), since in PD[111] the initial lifetime of minority charge carriers of the material is much higher, and the generation component of the dark current (I_d^G) is inversely proportional to the τ [11]:

$$I_d^G = e \frac{n_i}{2\tau} W_i A_{RE} \tag{1}$$

where n_i is own concentration of charge carriers in the substrate; e is the charge of the electron; A_{RE} is effective area of RE; W_i is space charge region (SCR) width.

It is also worth noting that curve 1 of *I-V* characteristic reaches saturation at U_{bias}=10-15 V, in contrast to curve 2, which reaches saturation at U_{bias}=70-80 V. This can be explained by the fact that the SCR of PD[100] stretches over the entire thickness of the substrate (not including the diffusion length of minority charge carriers) at lower bias voltages, since the PD[100] material has a much higher resistivity, and the W_i is directly proportional to the ρ [18]:

$$W_i = \frac{\sqrt{\rho U_{bias}}}{3} \times 10^{-4} \tag{2}$$

It should be added that in some samples of the PD[100] type, an increase in the dark current was observed with an increase in the reverse bias voltage over the entire measurement range (curve 3 of Fig. 3). To determine the reasons for the increase in dark current, it was decided to examine the surface of such PDs for surface structural defects. For this purpose, selective etching of the samples was performed (Fig. 4a, b). For comparison, PD[111] was also treated in a selective etchant (Fig. 4c, d).

It should be noted that in both cases studied, the silicon substrates were doped with the same phosphorus concentration in a single technological cycle. However, as can be seen from Fig. 4a, b, the surface of PD[111] had a much lower surface density of dislocations than PD[100]. The density of dislocations of PD[111] in the n^+-regions reached $N_{dis} \approx 2 \cdot 10^3$-$2 \cdot 10^3$ cm⁻², and in the p-regions $N_{dis} \approx 50$-90 cm⁻². In the case of the n^+-regions of PD[100], the determination of the dislocation density is complicated due to the high density of dislocations and the merging of their dislocation lines and grids, but it can be estimated that in this case $N_{dis} \approx 10^9$-10^{11} cm⁻². As for the p-regions of PD[100], in this case $N_{dis} \approx 1 \cdot 10^5$-$2 \cdot 10^5$ cm⁻². Note that the increased density of dislocations provokes an increase in the surface generation component of the dark current (I_d^{surf}) [19]:

$$I_d^{surf.} = \frac{e N_{ss} v_{drift} \sigma_{ss} A_{p-n}}{2}, \tag{3}$$

where σ_{ss} is capture cross-sectional area; N_{ss} – density of surface states; A_{p-n} - is the area that contributes to the surface component of the dark current; v_{drift} – is the average relative (relative to the center of re-combination) velocity of thermal charge carriers.

The influence of these defects and their number on I_d can be explained in several ways. First, the presence of dislocations can lead to the appearance of levels in the band gap due to the elastic stress fields associated with dislocations; these structural defects can serve as carrier recombination centers. The presence of recombination centers in the depleted region of the *p-n* junction will be manifested in an increase in the generation currents at the reverse bias on the PD. Secondly, dislocations can accumulate impurities due to their elastic fields. Decorated dislocations that cross the *p-n* junction lead to the appearance of a high density of generation-recombination centers in the spatial charge region. This again leads to an increase in the generation currents at the reverse bias [20, 21]. This situation was observed in some products of the PD$_{[100]}$ type.
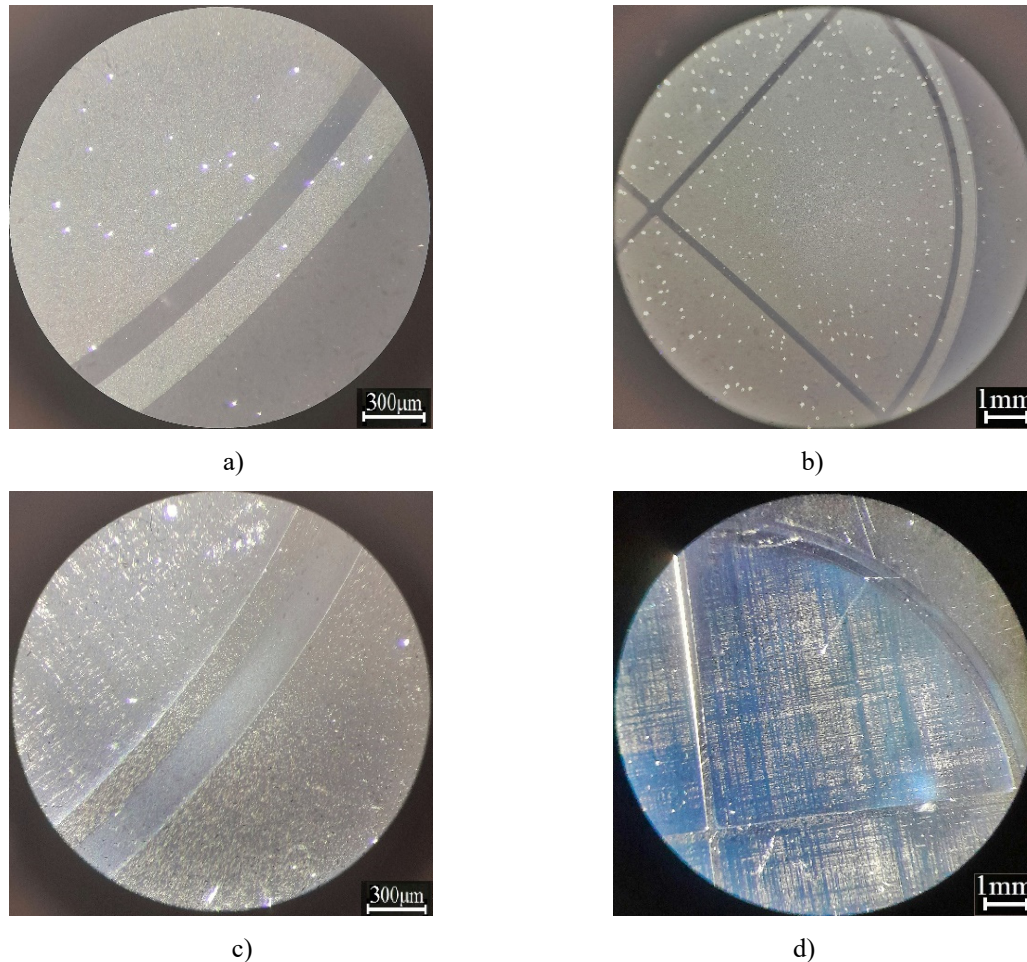

a)

b)

c)

d)

Figure 4. Image of the PD surface after selective etching in the dark field: a, b) PD$_{[111]}$; c, d) PD$_{[100]}$

We also investigated the value of the dark currents of the guard rings (J_{GR}). It was found that the dark current of the PD$_{[100]}$ guard ring was significantly higher than that of the PD$_{[111]}$. At U_{bias}=120 V J_{GR}=288-432 μA/cm^2 in PD$_{[100]}$ and J_{GR}=3.6-22 μA /cm^2 in PD$_{[111]}$. The increase in the guard ring currents in the case of PD$_{[100]}$ is caused by the presence of inversion channels at the interface between the Si-SiO$_2$ phases, which provokes an increase in currents when the SCR expands with an increase in the bias voltage.

B) Investigation of current monochromatic pulse responsivity of photodiodes.

The graph of $S_{pulse}(U_{bias})$ for both photodiode variants was obtained (Fig. 5). Figure 5 shows that the $S_{pulse}(U_{bias})$ dependence curve of PD$_{[100]}$ reaches saturation faster (at U_{bias}=7-9 V) than the PD$_{[111]}$ curve (at U_{bias}=70-80 V). This is due to the fact that in PD$_{[100]}$, as mentioned above, the SCR stretches to its maximum width at lower bias voltages, respectively, the charge carrier collection coefficient, which depends on W_i, reaches saturation also at lower U_{bias}, and the responsivity, being directly proportional to the charge carrier collection coefficient, also reaches saturation at lower bias voltages [22]:

$$S_\lambda = (1-R)TQ\alpha_{p-n}\frac{\lambda}{1.24},\qquad(4)$$

where R is the anti-reflective coating reflection coefficient; T is the transmission coefficient of the input window or optical filter; Q is the quantum output of the internal photoeffect; α_{p-n} is the collection coefficient of minor charge carriers generated by radiation in the active region of the photodiode.

Fig. 6a shows that the maximum of the spectral characteristic (S_m) of PD$_{[111]}$ shifts towards longer wavelengths with increasing bias voltage. This is caused by the expansion of the SCR with increasing reverse voltage, and when the W_i reaches saturation, no further shift of the maximum occurs. In the case of PD$_{[100]}$, a different picture was observed (Fig. 6b): even at low bias voltages, the maximum of the characteristic is at its maximum value of wavelenghts and does not shift with increasing voltage due to the high diffusion length of non-basic charge carriers and the maximum charge carrier collection coefficient even at two volts.
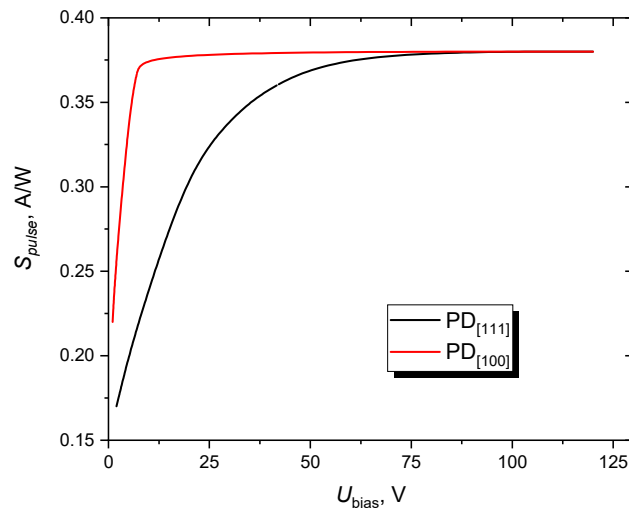

Figure 5. The graph of $S_{pulse}(U_{bias})$ PD$_{[100]}$ and PD$_{[111]}$

The spectral characteristics of the photodiode's responsivity are also obtained (Fig. 6).

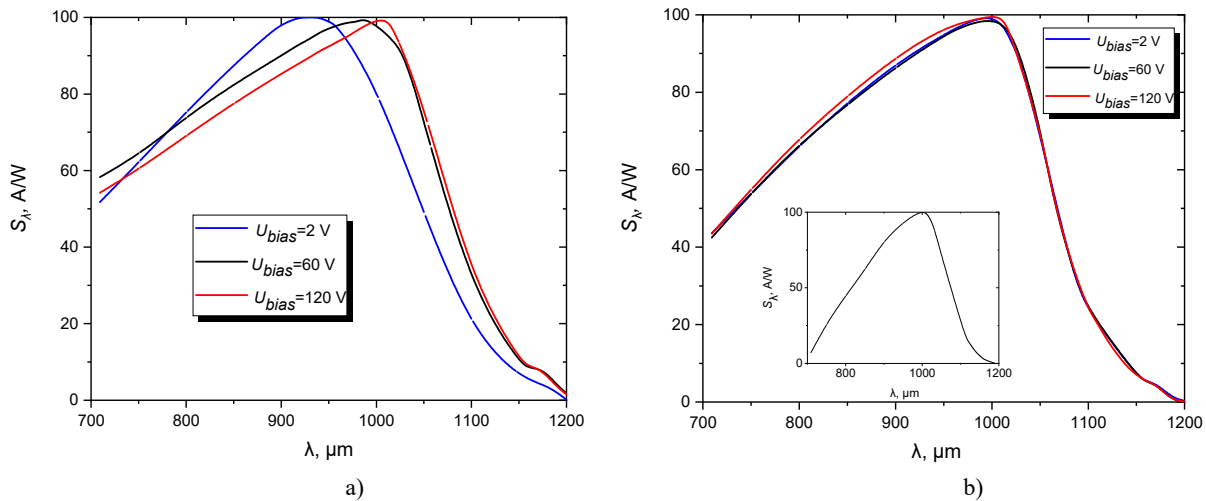a)   b)

Figure 6. Spectral characteristics of the photodiodes responsivity: a) PD$_{[111]}$; b) PD$_{[100]}$; inset in figure (b) is spectral characteristic of PD$_{[100]}$ with a short-wave minimum of the spectral characteristic of about $\lambda = 700$ nm

Note that in Fig. 6a and 6b the short-wave responsivity is different. For example, at $\lambda = 700$ nm, $S_\lambda = 0.5S_m$-$0.6S_m$ for PD$_{[111]}$, and for PD$_{[100]}$ $S_\lambda = 0.4S_m$. The change in the short-wave resistivity and the shift of the short-wave minimum of the spectral characteristic can be explained by the change in the depth of the n^+-p junction (x_{n+-p}). Indeed, when measuring the x_{n+-p}, it was seen that in PD$_{[111]}$ x_{n+-p} = 4-4.2 μm, and in PD$_{[100]}$ x_{n+-p} = 5.8-6 μm. Accordingly, as depth of the n^+-p junction decreases, the influence of background radiation and short-wave responsivity increases. This is due to the fact that with a decrease in the wavelength of radiation, the depth of its absorption decreases, and in p-i-n PDs, the formation of photocurrent occurs during the generation of charge carriers in the high-resistance p-region. And in the case of PD$_{[100]}$, a larger range of wavelengths is absorbed by the n^+-region due to the higher depth of the p-n junction. In particular, in some samples of the PD$_{[100]}$ type, a shift of the short-wave minimum of the spectral characteristic to 700 nm was observed (Fig.6b-inset). Note that the different depths of the diffusion layer in the two cases may be due to the difference in phosphorus diffusion coefficients for different crystallographic orientations.

B) Investigation of the growth rate of SiO₂ on the surface of different types of silicon

During the phosphor deposition operation, a anti-reflective SiO_2 is grown on the surface of the REs that meets the minimum reflection condition (5) [23]:

$$\frac{\lambda}{4} = nd_{SiO2}, \tag{5}$$

where λ is the working wavelength; n the refractive index of SiO_2; d_{SiO2} is the thickness of the anti-reflective film.

For the working wavelength of the described photodiodes, the anti-reflective oxide should be $d_{SiO2} \approx 0.18$-0.19 µm [24]. When studying the thickness of the grown anti-reflective oxide in the two studied variants of photodiodes, it was found that the thickness of SiO_2 in $PD_{[111]}$ reaches $d_{SiO2} \approx 0.183$ µm, and in $PD_{[100]}$ reaches $d_{SiO2} \approx 0.17$ µm. Presumably, the different growth rate of the oxide film is caused by the different surface concentration of silicon atoms (n) for different crystallographic orientations, since it can be assumed that the growth rate will increase with increasing surface concentration of atoms. To test this, we calculated the surface concentrations of silicon atoms for different crystallographic orientations. The surface concentration of atoms of different crystallographic planes of silicon can be visually estimated from Fig. 7a.

The surface concentration (the number of atoms per unit area) of atoms is calculated by the formula [25]:

$$n = \frac{N}{S}, \tag{6}$$

where N is the number of atoms that are completely contained in a unit cell of a two-dimensional surface lattice;

S is the area of the unit cell.

Let's calculate the value of n for plane (100). Plane (100) in the diamond structure is a two-dimensional square lattice with Si atoms in the nodes. The side of the square (the elementary cell of a two-dimensional lattice) is equal to half the diagonal of the face (Fig. 7b). A unit cell of the lattice contains one atom, since 1/4 of the atoms from each of the four atoms at the vertices of the square fall into the unit cell. So, the number of atoms per unit area of the plane (100) will be:

$$n_{(100)} = \frac{1}{\left(a\sqrt{2}/2\right)^2} = 6.78 \cdot 10^{14} \ cm^{-2} \tag{7}$$

where a is silicon lattice period.

For plane (111), the two-dimensional lattice is hexagonal (graphene structure). An elementary cell is a rhombus with side length a (angle 60°) and containing two Si atoms (Fig. 7b). Thus, the number of atoms per unit area of the plane (111) will be:

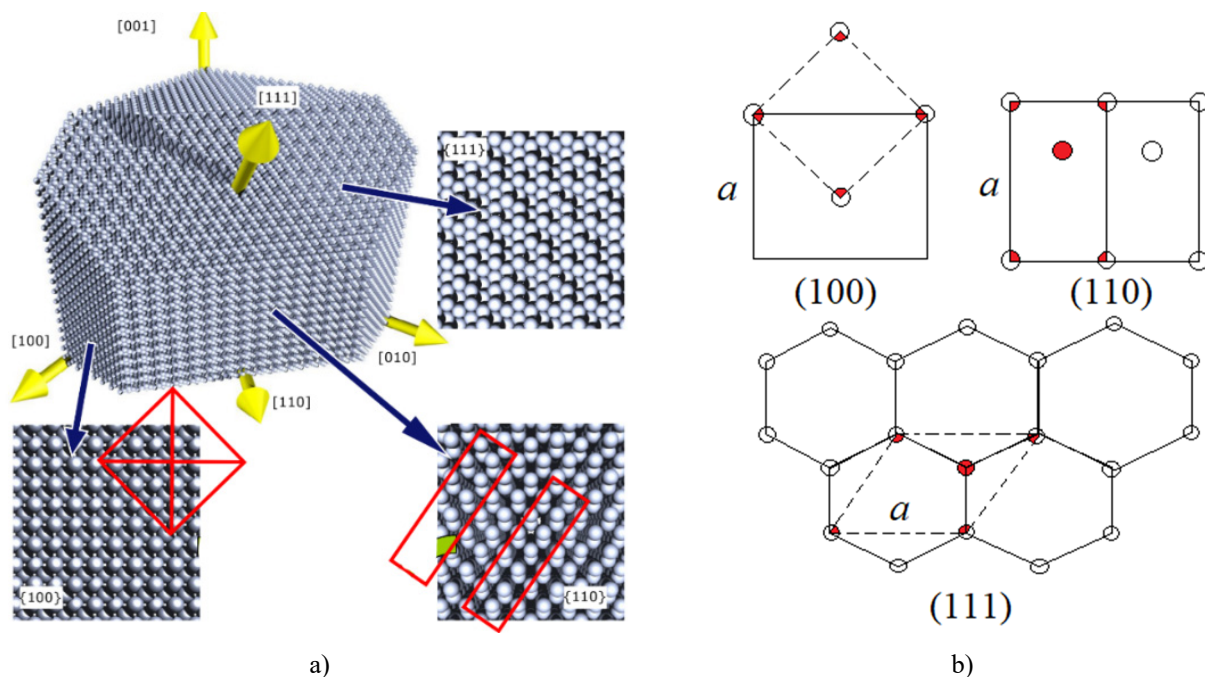$$n_{(111)} = \frac{1}{a^2\sqrt{3}/2} = 7.83 \cdot 10^{14} \ cm^{-2}. \tag{8}$$

Figure 7. A schematic representation of the density of silicon atoms inherent in different crystallographic planes: a) schematic illustration of an ingot; b) number of atoms in unit cells

For clarity, the surface density of silicon atoms for plane (110) is also shown. In the case of plane (110), a two-dimensional lattice is a rectangular lattice containing two atoms in a unit cell (Fig. 7b). The unit cell of the lattice is a

rectangle whose larger side is equal to the lattice constant a, and the other side is half the diagonal of the face of the elementary cube of the structure. Thus, the number of atoms per unit area of the plane (110) will be:

$$n_{(110)} = \frac{1}{a^2\sqrt{2}/2} = 9.59 \cdot 10^{14} \ cm^{-2}. \tag{9}$$

As can be seen from the calculations, the surface density of silicon atoms for different crystallographic planes is different, respectively, with an increase in the density of atoms, the growth rate of the oxide film increases.

As described in the paper, the final parameters of electronics elements, in particular photodiodes, depend on electrophysical parameters and the type of silicon used.

CONCLUSIONS

The influence of the electrophysical characteristics of silicon on the final parameters of photoelectronic elements on the example of *p-i-n* photodiodes is investigated. The following conclusions have been made:

1. Photodiodes made on the basis of silicon with a higher resistivity are more prone to the formation of inversion channels at the oxide-semiconductor interface. Samples with higher resistivity of the base material have lower insulation resistance between responsive elements.

2. The dark current and photosensitivity of such photodiodes reach saturation at a lower voltage.

3. Silicon-based photodiodes with a longer lifetime of non-basic charge carriers have lower values of dark currents.

4. Products with crystallographic orientation [111] have a much lower density of surface dislocations after technological operations than in the case of silicon with orientation [100].

5. Silicon of different crystallographic orientations has different phosphorus diffusion coefficients. This was established by determining the depth of charging of the diffusion layer of phosphorus at the same diffusion time.

6. Silicon oxide film grows faster on the surface of crystallographic orientation silicon [111] than on the surface of crystallographic orientation silicon [100]. This is due to the difference in the surface density of silicon atoms inherent in different crystallographic planes.

ORCID

Mykola S. Kukurudziak, https://orcid.org/0000-0002-0059-1387; **Volodymyr M. Lipka,** https://orcid.org/0009-0001-4419-3356

REFERENCES

[1] M.K. Bakhadyrkhanov, S.B. Isamov, Z.T. Kenzhaev, D. Melebaev, K.F. Zikrillayev, and G.A. Ikhtiyarova, Applied Solar Energy, **56**, 13 (2020). https://doi.org/10.3103/S0003701X2001003X

[2] H. Helmers, E. Lopez, O. Höhn, D. Lackner, J. Schön, M. Schauerte, and A.W. Bett, Physica status solidi – Rapid Research Letters, **15**(7), 2100113 (2021). https://doi.org/10.1002/pssr.202100113

[3] M. Kukurudziak, Radioelectronic and Computer Systems, **105**(1), 92 (2023). https://doi.org/10.32620/reks.2023.1.07

[4] A.V. Fedorenko, Technology and design in electronic equipment, **17**(3–4), 17 (2020). https://doi.org/10.15222/ TKEA2020.3-4.17 (in Ukrainian)

[5] W.J. Westerveld, M. Mahmud-Ul-Hasan, R. Shnaiderman, V. Ntziachristos, X. Rottenberg, S. Severi, and V. Rochus, Nature Photonics, **15(5)**, 341-345 (2021). https://doi.org/10.1038/s41566-021-00776-0

[6] A. Müller, M. Ghosh, R. Sonnenschein, and P. Woditsch, Materials Science and Engineering: B, **134**(2-3), 257 (2006). https://doi.org/10.1016/j.mseb.2006.06.054

[7] C. Ballif, F.J. Haug, M. Boccard, P.J. Verlinden, and G. Hahn, Nature Reviews Materials, **7**(8), 597 (2022). https://doi.org/10.1038/s41578-022-00423-2

[8] X. Pan, S. Li, Y. Li, P. Guo, X. Zhao, and Y. Cai, Minerals Engineering, **183**, 107600 (2022). https://doi.org/10.1016/j.mineng.2022.107600

[9] U. Hilleringmann, Wiesbaden: Springer Fachmedien Wiesbaden, 5-20 (2023). https://doi.org/10.1007/978-3-658-41041-4_2

[10] B. Son, Y. Lin, K.H. Lee, Q. Chen, and C.S. Tan, Journal of Applied Physics, **127**(20), 203105 (2020). https://doi.org/10.1063/5.0005112

[11] M.S. Kukurudziak, Journal of nano- and electronic physics, **14**(4), 04015 (2022). https://doi.org/10.21272/jnep.14(4).04015

[12] E. Sirtl, and A. Adler, Z. Metallk, **119**, 529 (1961).

[13] F.A. Abdullin, and V.E. Pautkin, in: *2019 IEEE International Seminar on Electron Devices Design and Production* (SED), 2023. https://doi.org/10.1109/SED.2019.8798467

[14] S.N. Knyazev, A.V. Kudrya, N.Y. Komarovskiy, Y.N. Parkhomenko, E.V. Molodtsova, and V.V. Yushchuk, Modern Electronic Materials, **8**(4), 131 (2022). https://doi.org/10.3897/j.moem.8.4.99385

[15] V.M. Lytvynenko, I.M. Vikulin, Bulletin of the Kherson National Technical University, (1), 46 (2018). (in Ukrainian)

[16] Yu.O. Kruglyak, and M.V. Strikha, Sensor Electronics and Microsystem Technologies, **16**(2), 5 (2019). https://doi.org/10.18524/1815-7459.2019.2.171224 (in Ukrainian)

[17] M.S. Kukurudziak, Journal of nano- and electronic physics, **14(1)**, 01023 (2022). https://doi.org/10.21272/jnep.14(1).01023

[18] V.A. Bruk, V.V. Garshenin, and A.I. Kurnosov, *Production of semiconductor devices: Textbook*. ed. 3rd, revision and supplement. (Vysshaya Shkola, Moscow, 1973). (in Russian)

[19] M.S. Kukurudziak, and E.V. Maistruk, Semicond. Sci. Technol., **38**, 085007 (2023). https://doi.org/10.1088/1361-6641/acdf14

[20] K. Ravey, *Defects and impurities in semiconductor silicon*, (Trans.), edited by G.N. Gorina, (Mir, Moscow, 1984). (in Russian).

[21] M.S. Kukurudziak, Semiconductor Physics, Quantum Electronics & Optoelectronics, **25**(4), 385 (2022). https://doi.org/10.15407/spqeo25.04.385

[22] V.P. Maslov, A.V. Sukach, V.V. Tetyorkin, M.Yu. Kravetskyi, N.V. Kachur, E.F. Wenger, and A.V. Fedorenko, Optoelectronics and Semiconductor Technology, **53**, 188 (2018). (in Ukrainian)

[23] S.B. Khan, S. Irfan, Z. Zhuanghao, and S.L. Lee, Materials, **12**(9), 1483 (2019). https://doi.org/10.3390/ma12091483

[24] M.S. Kukurudziak, East Eur. J. Phys. **2**, 289 (2023), https://doi.org/10.26565/2312-4334-2023-2-33

[25] P. Haas, F. Tran, and P. Blaha, Physical Review B, **79**(8), 085104. https://doi.org/10.1103/PhysRevB.79.085104

ВПЛИВ ХАРАКТЕРИСТИК КРЕМНІЮ НА ПАРАМЕТРИ ВИГОТОВЛЕНИХ ЕЛЕМЕНТІВ ФОТОЕЛЕКТРОНІКИ

Микола С. Кукурудзяк[a,b], Володимир М. Ліпка[a,b]

[a] АТ «Центральне конструкторське бюро Ритм», 58032, м. Чернівці, вул. Головна, 244, Україна

[b] Чернівецький національний університет імені Юрія Федьковича, 58002, м. Чернівці, вул. Коцюбинського, 2, Україна

В статті досліджено вплив електрофізичних характеристик кремнію на кінцеві параметри елементів фотоелектроніки на прикладі *p-i-n* фотодіодів. Під час досліджень встановлено, що зразки фотодіодів виготовлені на основі кремнію з вищим питомим опором більш схильні до утворенні інверсійних каналів на межі розділу оксид-напівпровідник. Також темновий струм та фоточутливість таких фотодіодів виходять в насичення при нижчій напрузі. Також побачено, що фотодіоди на основі кремнію із вищим часом життя неосновних носіїв заряду володять нижчими значеннями темнових струмів. Досліджено, що вироби із кристалографічною орієнтацією [111] володіють значно нижчою густиною поверхневих дислокацій після технологічних операцій, ніж в випадку кремнію з орієнтацією [100]. Також встановлено, що матеріал різної кристалографічної орієнтації має різні коефіцієнти дифузії фосфору. Експериментально встановлено що плівка оксиду кремнію росте швидше на поверхні кремнію кристалографічної орієнтації [111] , ніж на поверхні кремнію кристалографічної орієнтації [100]. Це спричинено відмінністю в поверхневій густині атомів кремнію притаманній різним кристалографічним площинам.

Ключові слова: *кремній; фотодіод; чутливість; темновий струм; дислокації; кристалографічна орієнтація*